

ural-parity-exchange contribution accounts for most of the observed strong energy dependence.

At 6 GeV/c and for $|t| < 1 \text{ GeV}^2$, the cross section ratio $\sigma(\pi^-p \rightarrow \varphi n)/\sigma(\pi^-p \rightarrow \omega n)$ is 0.0032 ± 0.0004 . In the quark model with no IOZ-rule breaking,¹¹ this ratio is equal to the fraction of nonstrange quarks in the φ , and gives a mixing angle (θ) of $38.5^\circ \pm 0.2^\circ$ for the vector mesons, compared to the ideal mixing angle of 35.3° and the values of $37.5^\circ \pm 0.3^\circ$ and $40.2^\circ \pm 0.3^\circ$ obtained from the linear and quadratic mass formulas,⁸ respectively. Since we have shown that φ and ω production by unnatural-parity exchange are quite dissimilar, it probably makes more sense to use the ratio of $|P_+|^2$, 0.0023 ± 0.0004 , which leads to $\theta = 38.0^\circ \pm 0.2^\circ$, a value clearly favoring the linear-over the quadratic-mass-formula value. This suppression factor of ~ 400 is similar to that observed in the IOZ-forbidden $f' \rightarrow \pi\pi$ decay relative to the allowed $f \rightarrow \pi\pi$ decay,^{3,9} and in the φ decay into $\rho\pi$.¹²

Further information on φ production is obtained from the $\langle Y_0^1 \rangle$ moment, which at these low masses is dominated by interference between P_0 and the S-wave amplitude, S_0 . By assuming a constant phase for S_0 throughout the φ region, fits to $\langle Y_0^1 \rangle$ for $|t| < 0.4 \text{ GeV}^2$ yield a phase for P_0 relative to S_0 of $-2^\circ \pm 7^\circ$ at the φ peak and a coherence between P_0 and S_0 of $\text{Re}(S_0^*P_0)/(|S_0||P_0|) = 0.61 \pm 0.10$ at the φ peak. These results show no significant t dependence. Insofar as the low-mass, low- $|t|$ S wave is due to π exchange³ (s-

channel nucleon helicity flip), our results imply a substantial helicity-nonflip contribution to the P_0 amplitude for φ production. The $\pi^-p \rightarrow \omega n$ data have also been interpreted^{7,13} in terms of a sizable nonflip exchange, the Z, with $J^{PC} = 2^{--}$. The rapid energy dependence of the unnatural-parity-exchange contribution to $\pi^-p \rightarrow \varphi n$ argues against a common origin for the large nonflip cross sections in the two reactions.

*Work supported by the U. S. Energy Research and Development Administration.

¹I. Iizuka, Prog. Theor. Phys., Suppl. **37-38**, 21 (1966); S. Okubo, Phys. Lett. **5**, 165 (1963); G. Zweig, CERN Report No. TH. 412, 1964 (unpublished).

²S. L. Kramer *et al.*, Phys. Rev. Lett. **33**, 505 (1974).

³A. J. Pawlicki *et al.*, ANL Report No. ANL-HEP-76-44 (to be published).

⁴A. J. Pawlicki *et al.*, Phys. Rev. D. **12**, 631 (1975).

⁵D. S. Ayres *et al.*, Phys. Rev. Lett. **32**, 1463 (1974).

⁶J. Pisut and M. Roos, Nucl. Phys. **B6**, 325 (1968).

⁷M. H. Shaevitz *et al.*, Phys. Rev. Lett. **36**, 8 (1976).

⁸T. G. Trippe *et al.*, Rev. Mod. Phys. **48**, No. 2, Pt. 2, S51 (1976).

⁹A. J. Pawlicki *et al.*, Phys. Rev. Lett. **37**, 971 (1976).

¹⁰E. L. Berger and C. Sorensen, Phys. Lett. **62B**, 303 (1976).

¹¹G. Alexander *et al.*, Phys. Rev. Lett. **17**, 412 (1966).

¹²R. Dashen and D. Sharp, Phys. Rev. **133**, B1585 (1964); J. Yellin, Phys. Rev. **147**, 1080 (1966). Recent branching ratios yield $g_{\varphi\rho\pi^2}/g_{\omega\rho\pi^2} \sim 0.0036$ (Dashen and Sharp) and ~ 0.0022 (Yellin).

¹³A. C. Irving, Nucl. Phys. **B105**, 491 (1976).

Fission Barriers at High Angular Momenta*

M. Beckerman and M. Blann

Department of Chemistry and Nuclear Structure Research Laboratory,†
University of Rochester, Rochester, New York 14627

(Received 18 November 1976)

Fission and evaporation-residue excitation functions for 170–340-MeV $^{40}\text{Ar} + ^{109}\text{Ag}$ have been analyzed with a code which treats multiple-particle emission with explicit angular-momentum dependence. It is found that the liquid-drop barriers must be reduced by 40% to reproduce experimental results, and that multiple-chance fission contributions are essential to the analysis.

Heavy-ion-induced fission excitation functions provide valuable data for analysis of nuclear deformations at high angular momenta since (in nuclei of $A \lesssim 200$) fission results predominantly from high-angular-momentum states. The extraction of information depends upon unfolding by means of model calculations; and many of the analyses

performed to date have been based upon erroneous or highly questionable procedures. For example, (a) the entire reaction cross sections or arbitrary constant fractions have been used to give the compound-nucleus spin distributions¹; (b) statistical analyses have been applied without using spin-dependent level densities^{1,2} (in other

than an s-wave approximation); and (c) the arbitrary assumption has been made that only first-chance fission need be considered.¹ These shortcomings assure that parameters derived from such analyses vary between being questionable at best, to incorrect.

In this Letter we report analyses of fission and evaporation-residue excitation functions for the system $^{40}\text{Ar} + ^{109}\text{Ag}$ at laboratory bombarding energies between 170 and 340 MeV. We use explicit spin-dependent level densities for particle emission and fission, with allowance for multiple-

chance fission. We use the Bohr-Wheeler model³ with rotational energies based upon the rotating-liquid-drop model (RLDM),⁴ and find an interesting and unexpected result for the barriers required to reproduce the experimental results. We show that the simultaneous fitting of fission and evaporation excitation functions using experimental l_{crit} values is necessary to remove ambiguities from the parameter choices, and that neglect of multiple-chance fission in such calculations is not justified.

The fission and particle-emission widths used in this work are represented by

$$\Gamma_f \propto (2I+1) \int_0^{E-E_{\text{sp}}(I)} \rho_f [E - E_{\text{sp}}(I) - k] dk, \quad (1)$$

$$\Gamma_\nu \propto (2S_\nu + 1) \sum_{l=0}^{\infty} \sum_{J=|I-l|}^{I+l} (2J+1) \int_0^{E-E_{\text{min}}(J)-B_\nu} \rho_\nu [E - E_{\text{min}}(J) - B_\nu - \epsilon] T_\nu^l(\epsilon) d\epsilon,$$

where symbols are defined in Table I. There are two adjustable parameters in the model, a_f/a_ν and B_f . Rotational energies for the ground state at equilibrium deformation and for the nucleus at the saddle point (versus I) were evaluated from the RLDM, where the barrier scaling parameter enters as

$$E_{\text{sp}}(I) = E_{\text{min}}(I) + B(I)B_f. \quad (2)$$

A computer code was written to evaluate the fission and particle-emission widths for all elements of the E - J plane for each nuclide in the de-excitation chain.⁶ The logic used in evaluating

the decay widths for each population element of the E - J plane has been described previously⁷; a grid size of 1 MeV by $1\hbar$ is used.

We have chosen the $^{40}\text{Ar} + ^{109}\text{Ag}$ data⁸ for testing the model since these data provide both evaporation-residue and fission excitation functions over a broad bombarding-energy range corresponding to excitation energies of 70–190 MeV and critical angular momenta for fusion, l_{crit} , of $(50\text{--}100)\hbar$. The comparisons to be presented clearly show the necessity of having both sets of data over a broad dynamic range: The small fission cross

TABLE I. Definition of symbols.

Γ_f, Γ_ν	Fission and particle-emission widths.
I, J	Emitting- and residual-nucleus angular momenta.
S_ν, B_ν	Intrinsic spin and binding energy of particle ν (with $\nu = n, p$, or α).
$T_\nu^l(\epsilon)$	Transmission coefficient for kinetic energy ϵ and orbital angular momentum l , obtained from the optical model with widely used optical-model parameters for neutrons, ^a protons, ^b and α particles. ^c
ρ_f, ρ_ν	Level densities at fission saddle point and for particle emission; $\rho \propto U^{-2} \exp(2 \times \sqrt{a}U)$ where, following Lang (Ref. 5), the angular-momentum dependence is due to adjustment of the excitation energy for an appropriate rotational energy [see Eq. (1)].
a_f, a_ν	Single-particle level densities at fission saddle point and equilibrium deformation; used in ρ_f and ρ_ν with $a_\nu = A/10$.
$B(I)$	Rotating-liquid-drop fission barrier at angular momentum I .
B_f	Scaling parameter to adjust the fission barriers [see Eq. (2)].
$E_{\text{min}}(I)$	Rotational energy for a nucleus at angular momentum I and equilibrium deformation from RLDM (Ref. 3).
$E_{\text{sp}}(I)$	Rotational energy of a nucleus with angular momentum I at the saddle-point deformation, from RLDM (Ref. 3) or modified as in Eq. (2).
E	Excitation energy in the emitting (fissioning) nucleus.

^aF. G. Perey and B. Buck, Nucl. Phys. **32**, 353 (1962).

^bF. G. Perey, Phys. Rev. **131**, 745 (1963).

^cG. R. Satchler, Nucl. Phys. **70**, 177 (1965).

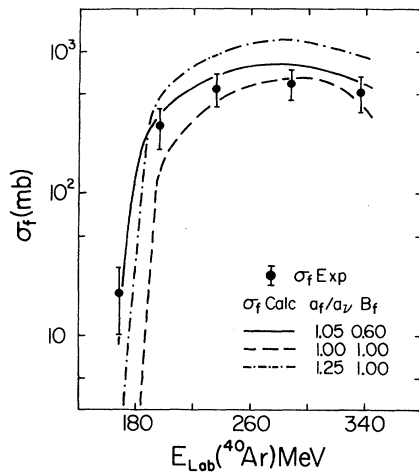


FIG. 1. Experimental and calculated fission cross sections. Filled circles denote data from Ref. 8. The three sets of curves show calculated cross sections obtained with combinations of the parameters a_f/a_ν and B_f as indicated.

sections near threshold set one requirement; the evaporation residues permit restrictions at the higher bombarding energies, independent of any uncertainties as to whether or not some major portion of the reported fission cross sections is equilibrium fission or quasifission.

In Fig. 1 the experimental fission excitation functions are compared with three representative sets of calculated values with the following parameter choices: (a) $a_f/a_\nu = 1.00$, $B_f = 1.00$; (b) $a_f/a_\nu = 1.25$, $B_f = 1.00$; and (c) $a_f/a_\nu = 1.05$, $B_f = 0.60$. It may be seen that the requirement set by the threshold fission cross sections eliminates sets (a) and (b); set (b) also leads to the near disappearance of the calculated high-energy evaporation residues (see, e.g., column 5 of Table II), and further increases in a_f/a_ν to improve the threshold fission agreement are thereby ruled out. The excitation-function fitting can be accomplished by also varying B_f ; and a good parameter set is represented by (c). It is shown in Table II that set (c) leads to high-energy evaporation residues in good agreement with the experimental values (the fitting to high-energy evaporation residues is independent of whether some fraction of the highest partial waves assumed to undergo fission are, in fact, quasifission, as discussed in Ref. 2). In Table II, a finer parameter mesh size and broader range of parameter values are presented to illustrate the points just stated, and to give some better idea as to the sensitivity of calculated results to small parameter varia-

TABLE II. Comparison of experimental fission and evaporation-residue cross sections (Ref. 8) with results calculated with the listed combinations of the parameters a_f/a_ν and B_f (present work).

a_f/a_ν	B_f	$\sigma_f(169)$ (mb)	$\sigma_{er}(236)$ (mb)	$\sigma_{er}(337)$ (mb)
1.00	1.00	0.005	710	530
1.15	1.00	0.25	480	240
1.30	1.00	4.7	330	< 1
1.26	0.90	9.1	210	< 1
1.19	0.80	9.4	280	140
1.12	0.70	9.4	380	180
1.05	0.60	10	480	370
0.98	0.50	16	580	660
		20 ± 10^a	620 ± 80^a	455 ± 50^a

^a Experimental data (Ref. 8).

tions. We feel that the data are best described by a parameter set given by $B_f = 0.60 \pm 0.05$ and $a_f/a_\nu = 1.03 \pm 0.03$.

Some theoretical support for a reduction in the liquid-drop barriers may be found in a model using a liquid drop with finite range,⁹ in which barriers were found in the mass-150 region corresponding to $B_f = 0.8-0.9$. The results implied by our work represent reductions of $E_{sp}(I)$ from the pure-liquid-drop results of 4.7 MeV for $I=60$, and 2.1 MeV for $I=70$; the corresponding percentage reductions in the saddle-point energies

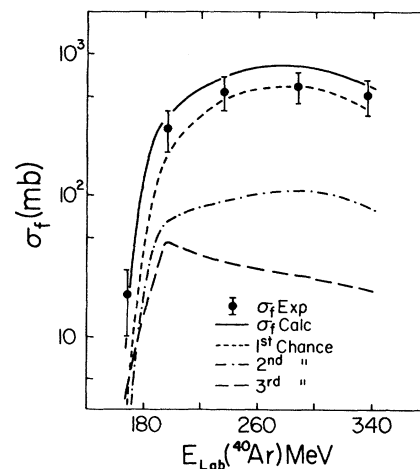


FIG. 2. Experimental and calculated fission cross sections. Filled circles denote data from Ref. 8; solid curve, results calculated with $a_f/a_\nu = 1.05$ and $B_f = 0.60$. First-, second-, and third-chance fission components of the total calculated fission cross sections are individually indicated.

are 12% and 5%, respectively. Some of the discrepancy can be understood to be due to the finite-range effect⁹; the difference may well be within the range expected for shell effects in highly deformed nuclei.¹⁰

The relative importance of multiple-chance fission contributions to the total fission excitation function calculated with parameter set (c) is exhibited in Fig. 2. The principal multiple-chance fission components are displayed. In the threshold region, multiple-chance fission is dominant; and at 169 MeV, the contributions due to first-through fourth-chance fission are 2.5, 1.4, 3.8, and 2.5 mb, respectively. The relative importance of multiple-chance fission decreases with increasing excitation energy, although at 337 MeV the multiple-chance contribution is still 33% of the total.

To summarize: (1) It is necessary to fit fission and evaporation-residue excitation functions simultaneously over a broad excitation-energy range and to use experimental l_{crit} values in order to obtain unambiguous model parameters. (2) The assumption that only first-chance fission need be considered in such analyses is a poor one for the parametrization considered herein. (3) A reduction in the liquid-drop barriers on the order of 35–45% is necessary to reproduce the experimental excitation functions in the mass-150 region.

*Work supported in part by the U. S. Energy Research and Development Administration.

†Supported by the National Science Foundation.

¹T. Sikkeland, Phys. Rev. **135**, B699 (1964); T. Sikkeland, J. E. Clarkson, N. H. Steiger-Shafir, and V. E. Viola, Phys. Rev. C **3**, 329 (1971).

²M. Blann and F. Plasil, Phys. Rev. Lett. **29**, 303 (1972); F. Plasil and M. Blann, Phys. Rev. C **11**, 508 (1975); see M. Blann, U. S. ERDA Reports No. COO-3494-29 and No. COO-3494-32 (unpublished) for a description and revisions of the overlaid ALICE code.

³N. Bohr and J. A. Wheeler, Phys. Rev. **56**, 426 (1939).

⁴S. Cohen, F. Plasil, and W. J. Swiatecki, Ann. Phys. (N.Y.) **82**, 557 (1974).

⁵D. W. Lang, Nucl. Phys. **77**, 545 (1966).

⁶See M. Beckerman and M. Blann, University of Rochester Nuclear Structure Research Laboratory Report No. UR-NSRL-135 (unpublished) for a description of MB-II.

⁷M. Blann, Phys. Rev. **157**, 860 (1967).

⁸H. C. Britt, B. H. Erkkila, R. H. Stokes, H. H. Gutbrod, F. Plasil, R. L. Ferguson, and M. Blann, Phys. Rev. C **13**, 1483 (1976).

⁹H. J. Krappe and J. R. Nix, in *Proceedings of the Third International Atomic Energy Symposium on the Physics and Chemistry of Fission* (International Atomic Energy Agency, Vienna, 1974), Vol. I, p. 159.

¹⁰Z. Szymanski, private communication, and in *Proceedings of the International Symposium on Highly Excited States in Nuclei, 23–26 September 1975, Jülich, W. Germany*, edited by A. Faessler, C. Mayer-Böricke, and P. Turek (Kernforschungsanlage Jülich GmbH, Jülich, Federal Republic of Germany, 1975), p. 34.

Pulse Fourier-Transform Optical Spectroscopy*

Stephen B. Grossman, A. Schenzle, and Richard G. Brewer

IBM Research Laboratory, San Jose, California 95193

(Received 14 December 1976)

The optical analog of pulse Fourier-transform NMR spectroscopy is demonstrated. Doppler-free infrared spectra are obtained for a set of closely spaced $^{13}\text{CH}_3\text{F}$ transitions at $9.66\ \mu\text{m}$ from two-pulse echo and free-induction decay transients. The effects of elastic or inelastic collisions on the decay rate are obtained for each transition, and the long-range force laws are deduced from the dependence of the scattering cross section on molecular velocity.

The method of Fourier transforming transient phenomena from the time to the frequency domain has proven to be an extremely versatile technique in pulsed nuclear-magnetic-resonance (NMR) spectroscopy.¹ With it, ultrahigh-resolution NMR spectroscopy can be performed quickly and with high sensitivity in a set of densely spaced lines.² Since the NMR signals display coherent transient behavior, dynamic information about nuclear spin

interactions can be derived in a selective manner for each transition as well.³

This Letter reports an initial demonstration of this Fourier-transform technique in the optical region. By employing suitable coherent optical transient effects in a sample of $^{13}\text{CH}_3\text{F}$, we are able to resolve Doppler-free spectra in a set of closely spaced lines (Fig. 1). The decay characteristics for each transition are obtained also and